The oocyte zinc transporter *Slc39a10/Zip10* is a regulator of zinc sparks during fertilization in mice.

Atsuko Kageyama[1], Narumi Ogonuki[2], Takuya Wakai[3], Takafumi Namiki[1,4], Yui Kawata[1], Manabu Ozawa[5], Yasuhiro Yamada[6], Toshiyuki Fukada[7], Atsuo Ogura[2], Rafael A. Fissore[8], Naomi Kashiwazaki[1,9], Junya Ito[1,9,10*]

[1] Laboratory of Animal Reproduction, School of Veterinary Medicine, Azabu University, Sagamihara, 252-5201, Japan.

[2] Bioresource Engineering Division, Bioresource Research Center, RIKEN, Tsukuba, 305-0074, Japan.

[3] Department of Animal Science, Graduate School of Environmental and Life Science, Okayama University, Okayama, 700-8530, Japan.

[4] Present address: Department of Life Science Frontiers, Center for iPS Cell Research and Application (CiRA), Kyoto University, Kyoto, 606-8507, Japan.

[5] Laboratory of Reproductive Systems Biology, Center for Experimental Medicine and Systems Biology, The Institute of Medical Science, The University of Tokyo, Minato-ku 108-8639, Japan.

[6] Department of Molecular Pathology, Graduate School of Medicine, The University of Tokyo, Bunkyo-ku 113-0033, Japan.

[7] Laboratory of Molecular and Cellular Physiology, Faculty of Pharmaceutical Sciences, Tokushima Bunri University, Tokushima 770-8514, Japan.

[8] Department of Veterinary and Animal Sciences, University of Massachusetts Amherst, Amherst 01003-9292, the United States.

[9] Graduate School of Veterinary Science, Azabu University, Sagamihara, 252-5201, Japan.

[10] Center for Human and Animal Symbiosis Science, Azabu University, Sagamihara, 252-5201, Japan.

*Correspondence:

Junya Ito, Laboratory of Animal Reproduction, Graduate School of Veterinary Sciences, Azabu University, Sagamihara, 252-5201, Japan, itoj@azabu-u.ac.jp

Abstract

In all vertebrates studied to date, a rise(s) in intracellular calcium is indispensable for successful fertilization and further embryonic development. Recent studies demonstrated that zinc is ejected to the extracellular milieu, the 'zinc spark', and

follows the first few calcium rises of fertilization. However, the role of the zinc sparks in fertilization and development, and the supporting influx mechanism(s) are unknown. In this study, we focused on zinc transporters *Zip10/Slc39a10* which was expressed in mouse oocytes through follicular development, and investigated the oocyte-specific deficient mice for *Zip10* (*Zip10*$^{d/d}$: *Zip10*$^{flox/flox}$ *Gdf9*$^{Cre/+}$). *Zip10* mRNA or ZIP10 protein was expressed throughout folliculogenesis in the oocyte or plasma membrane, respectively. The number of ovulated oocytes was examined in *Zip10*$^{d/d}$ mice, and no change from the number of oocytes was observed. *Zip10*$^{d/d}$ oocytes decreased zinc level in the oocytes, but did not affect maturation and metaphase II spindles formation. Fertilization-induced calcium oscillations were present in *Zip10*$^{d/d}$ oocytes, but zinc sparks were not observed. Despite other events of egg activation proceeding normally in *Zip10*$^{d/d}$ oocytes, embryo development into 4-cells and beyond was compromised. We show here for the first time that the zinc transporter ZIP10 contributes to zinc homeostasis in oocytes and embryos, highlighting the role of labile zinc ions in early development.

Submission information

The zinc transporter, *Slc39a10/Zip10*, is required for the zinc sparks of fertilization in mice.

Introduction

In mammalian fertilization, the sperm factor is released into the ooplasm to activate the oocyte (Yoon and Fissore, 2007). It is now believed that phospholipase C zeta (PLCζ) (Yoon and Fissore, 2007; Saunders et al., 2002) is the sperm factor and it induces in the ooplasm repetitive increases in the intracellular Ca^{2+}, termed 'calcium oscillations.' These oscillations play an essential role in triggering the oocyte activation events, such as cortical granule exocytosis, the block of polyspermy, meiotic resumption and exit from MII arrest (Xu et al., 1994; Jones, 2005; Ducibella et al., 2006; Ito et al., 2011; Sugita et al.,

2024). A calcium increase is highly conserved in many species as the trigger of egg activation and is vital for successful fertilization.

In recent years, zinc ions as well as calcium ions, are thought to play important roles during fertilization (Suzuki et al., 2010; Allouche-Fitoussi and Breitbart, 2020; Kageyama et al., 2022). Zinc ion is an essential trace element and the second most abundant transition ion in the human body after iron (Lubna and Ahmad, 2023). Zinc homeostasis is essential for optimal metabolic function in the reproductive process in mammals (Pascua et al, 2020), therefore zinc deficiency causes abnormalities such as fetal teratogenicity, long gestation periods, problematic labor, low birth weight and weak offspring (Favier, 1992; Bedwal and Bahuguna, 1994). Zinc also has important role in the male and female germ cells (Allouche-Fitoussi and Breitbart, 2020; Kageyama et al., 2022). Especially in the mouse female germ cells, zinc-deficient condition caused profound defects in oocyte maturation, cumulus cell expansion and ovulation cycle (Tian and Diaz, 2012). Several studies have been conducted in mice to understand how zinc regulates oocyte maturation. Zinc was reported to be a critical regulator of meiosis throughout oocyte maturation, including maintaining release from the first and second meiotic arrest (Kong et al., 2012). In addition, zinc levels of oocytes were found to increase by 50% as the oocyte progressed through meiosis (Kim et al., 2010; Bernhardt et al., 2011).

In 2011, Kim *et al*. reported the importance of zinc during mammalian fertilization (Kim et al., 2011). Zinc is predominantly stored in vesicles that are symmetrically arranged along the oocyte cortex at the GV stage, and zinc-stored vesicles (cortical granules) are located away from the spindle and form a hemispherical pattern at the MII stage (Kim et al., 2011; Que et al., 2015; Kong et al., 2014; Que et al., 2019; Jo et al., 2019; Que et al., 2017). After the penetration of sperm, it has been induced a ‘zinc spark’ that releases billions of labile zinc ions from the cortical granules, and the total zinc content of the oocytes decreases by 10-20% in at the end of fertilization in mice (Kim et al., 2011; Lee et al., 2020). In addition, these events immediately follow a series of calcium oscillations (Kim et al., 2011). Zinc spark has also been observed in the cattle, non-human primate, human and Xenopus laevis oocytes (Kim et al., 2011; Que

101 et al., 2019; Duncan et al., 2016; Seeler et al., 2021), suggesting that this
102 phenomenon is a highly conserved event in vertebrate. More surprisingly, full-
103 term development of mouse embryos has been reported by chelation of Zn^{2+} ions
104 without Ca^{2+} release, suggesting the depletion of zinc ions in oocytes may be
105 sufficient for oocyte activation(Suzuki et al., 2010). Zinc has also been reported
106 to impact the sperm during fertilization in mice. Zinc accumulation in the zona
107 pellucida increases fibril binding along the glycoprotein matrix and decreases the
108 number of sperm that can reach the fertilized oocytes (Que et al., 2017; Aonuma
109 et al., 1981; Tokuhiro and Dean, 2018). After the zinc sparks, the released zinc
110 affects the forward motility of sperm to prevent their passage through the zona
111 matrix (Tokuhiro and Dean, 2018). Zinc spark is associated with the release of
112 ovastacin (*Astl*, the official gene name), which is required for the zona reaction,
113 and functions as a polyspermy block mechanism that is initiated only a few
114 minutes after fertilization (Tokuhiro and Dean, 2018).

115 The transport of zinc ions into and out of cells is regulated by zinc
116 transporters. In mammals, 14 zinc ion importers, called as ZIP (ZIP1-ZIP14),
117 have been identified (Fukada and Kambe, 2011; Takagishi et al., 2017; Kambe
118 et al., 2015). Previous study showed that mammalian oocytes regulate zinc
119 uptake through two maternally derived and cortically distributed zinc transporters,
120 ZIP6 and ZIP10 (Kong et al., 2014). Further, they reported that targeted disruption
121 using *Zip6*- and *Zip10*- specific morpholino injection or antibody incubation
122 induced alteration of the intracellular labile zinc content, spontaneous resumption
123 of meiosis from the PI arrest and premature arrest at a telophase I-like state
124 (Kong et al., 2014). It is clear from these reports that ZIP6 and ZIP10 are involved
125 in zinc transport in oocytes, but the function is not elucidated.

126 In this study, we generated oocyte specific *Zip6* and *Zip10* conditional
127 knockout mice and examined the function of ZIP10 in the oocytes and the
128 importance of zinc homeostasis during fertilization and embryonic development.
129 This study provides clues that elucidate its role in fertilization and embryonic
130 development, which is still largely unknown. In addition, this is the first report
131 confirming the function of the zinc transporter in oocytes, which will contribute to
132 future research.

133

134 **Results**

135 **Zinc transporters, ZIP6, and ZIP10, are expressed in mouse oocytes**
136 **through follicular development**

137 First, using *in situ* hybridization and immunofluorescent staining, we
138 examined the expression of ZIP10 during follicular development. As shown in Fig.
139 1A, *Zip10* mRNA was expressed from the primordial oocyte (Arrow). It continued
140 to be expressed in oocytes of primary, secondary, and antral follicles. ZIP10
141 protein was also expressed in the plasma membrane of primordial oocytes
142 (Fig.1B; Arrow). We also confirmed the expression of ZIP10 protein at the plasma
143 membrane of oocytes of primary, secondary, and antral follicles. Although ZIP6
144 was also expressed in oocytes throughout folliculogenesis (Fig.1C; Arrow), it
145 displayed nuclear localization in oocytes and granulosa cells of primary,
146 secondary, and antral follicles. Fig. 1D showed zona pellucida and granulosa
147 cells through the follicular development.

148

149 **Phenotype of oocyte-specific *Zip6*$^{d/d}$ and *Zip10*$^{d/d}$ female mice.**

150 To elucidate the roles of *Zip6* and *Zip10* in the mouse oocytes, oocyte-
151 specific *Zip6* (*Zip6*$^{d/d}$) and *Zip10* (*Zip10*$^{d/d}$) knockout mice were generated (Fig.
152 S1A-C). We examined whether ZIP6 and ZIP10 protein expression was absent
153 in *Zip6*$^{d/d}$ and *Zip10*$^{d/d}$ oocytes (Fig. S1D). *Zip6*$^{f/f}$ and *Zip10*$^{f/f}$ mice were used as
154 controls, respectively. We examined the number of ovulated oocytes or defects
155 in oocyte maturation. After superovulation, the number of ovulated oocytes
156 collected from the oviduct in *Zip10*$^{d/d}$ mice was 22.1 ± 2.5 oocytes/mouse (Fig.
157 2A), which was equivalent to that in *Zip10*$^{f/f}$ mice (18.7 ± 2.9 oocytes/mouse, $p >$
158 0.05). The numbers of ovulated oocytes in *Zip6*$^{d/d}$ and *Zip6*$^{f/f}$ mice were also
159 equivalent (28.7 ± 3.6 and 32.8 ± 3.3 oocytes/mice, respectively, $p > 0.05$) (Fig.
160 S2A). As for oocyte maturation, the rate of oocytes with a first polar body at 10h,
161 12h, and 14h in the *Zip10*$^{d/d}$ group was not different than that of *Zip10*$^{f/f}$ group
162 (*Zip10*$^{d/d}$: 58.7%, 61.9%, and 79.4%, *Zip10*$^{f/f}$: 50.8%, 54.1% and 70.5%,
163 respectively, $p > 0.05$, Fig. 2B). In addition, *Zip10*$^{d/d}$ oocytes display intact
164 metaphase spindles just as in the *Zip10*$^{f/f}$ groups (Fig. 2C).

165 Next, we examined the levels of labile zinc in germinal vesicle (GV), MII,
166 and two pronuclei (2PN) zygotes by comparing the fluorescence intensity
167 following loading with the dye, FluoZin-3AM (Fig. 2D). The FluoZin-3AM
168 fluorescence intensity in GV and MII oocytes of the *Zip10*$^{d/d}$ group was lower than
169 the *Zip10*$^{f/f}$ group ($p < 0.05$). After fertilization, the fluorescence intensity in *Zip10*$^{f/f}$
170 zygotes decreased dramatically, and also decreased for the *Zip10*$^{d/d}$ group,
171 although it remained higher than for *Zip10*$^{f/f}$ oocytes. When compared within
172 group, the fluorescence intensity in *Zip10*$^{f/f}$ between GV and MII oocytes was
173 significantly different (GV vs. MII and MII vs 2PN; $p < 0.05$, respectively), but the
174 stages of *Zip10*$^{d/d}$ oocytes were not different despite clear trends ($p > 0.05$). The
175 levels of zinc fluorescence intensity in the *Zip6*$^{d/d}$ group were not different from
176 the controls *Zip6*$^{f/f}$, which decreased markedly at fertilization (Fig. S2B; $p > 0.05$).
177

178 **The zinc sparks of *Zip10*$^{d/d}$ oocytes were suppressed after fertilization or**
179 **artificial activation.**

180 To determine if the absence of ZIP6 and ZIP10 influenced the detection of
181 Zn^{2+} sparks associated with fertilization, we monitored extracellular zinc and
182 intracellular calcium during fertilization of *Zip6*$^{d/d}$ and *Zip10*$^{d/d}$ oocytes (Fig. S3
183 and 3A). *Zip10*$^{f/f}$ oocytes displayed the expected calcium oscillations following
184 fertilization, and a zinc spark followed the first calcium rise (Fig. 3A upper side,
185 movies 1 and 2). In contrast, *Zip10*$^{d/d}$ oocytes did not release zinc ions
186 immediately after the first calcium spike, despite mounting normal calcium
187 oscillations (Fig. 3A lower side, movies 3 and 4). In *Zip6*$^{d/d}$ oocytes, a zinc spark
188 occurred immediately after the first intracellular calcium rise at fertilization, just as
189 in control *Zip6*$^{f/f}$ oocytes (Fig. S3, movie S1-S4). The extracellular zinc sparks
190 were examined following artificial oocyte activation of mouse oocytes with
191 ionomycin. The zinc sparks occurred immediately after the intracellular calcium
192 rise in *Zip10*$^{f/f}$ oocytes (Fig. 3B upper side, movies 5 and 6), however, *Zip10*$^{d/d}$
193 oocytes did not release zinc ions after the calcium spike (Fig. 3B lower side,
194 movies 7 and 8).
195

196 ***Zip10*$^{d/d}$ mouse oocytes can be fertilized but were unlikely to develop to the**

197 **blastocysts.**

198 *Zip6*$^{d/d}$ and *Zip10*$^{d/d}$ oocytes then were used for IVF, and we examined the
199 rates of fertilization, polyspermy, and embryo development. Successful
200 fertilization was confirmed at 6 h after IVF by the presence of pronuclei (Fig. 4A
201 and B). *Zip10*$^{d/d}$ oocytes were fertilized at rates like those observed for control
202 oocytes (Fig. 4A). Consistent with this, the zona reaction triggered by fertilization
203 and examined using a ZP2 antibody was similar in *Zip10*$^{d/d}$ and *Zip10*$^{f/f}$ oocytes
204 (Fig. 4D). We also examined the localization of ovastacin, whose expression in
205 the cortex and loss post-fertilization was comparable between the two groups (Fig.
206 4E). As for the expression of JUNO, it had the same expression than between
207 null and control oocytes (Fig. S4) and the temporal dynamics of its disappearance
208 from the cortex after fertilization was similar for both *Zip10*$^{f/f}$ and *Zip10*$^{d/d}$ groups
209 (Fig. 4F).

210 We next examined the development to the blastocyst stage, and whereas
211 *Zip10*$^{f/f}$ zygotes developed at the expected rates, approximately 78.9% (2 cell),
212 90.3 (4-8 cell) and 75.0% (blastocyst), a smaller fraction of *Zip10*$^{d/d}$ zygotes did
213 37.2% (2 cell) and 38.3% (4-8 cell) and only 32.7% reached blastocyst stage (p
214 < 0.05; Fig. 4B). As shown in Fig. 4C, the total cell numbers of blastocysts were
215 also lower for *Zip10*$^{d/d}$ embryos (51.6 ± 2.1 cells) than for those of *Zip10*$^{f/f}$ ones
216 (72.7 ± 2.1 cells, $p < 0.05$). *Zip6*$^{d/d}$ oocytes did not display any alterations in the
217 rate of fertilization or development (Fig. S2C and D; $p > 0.05$).

218

219 **Discussion**

220 The zinc sparks associated with fertilization were first discovered in the
221 mouse (Kim et al., 2011). Similar observations followed in other mammalian
222 species and amphibians (Que et al., 2019; Duncan et al., 2016; Seeler et al.,
223 2021). However, the underlying mechanism(s) and biological role of zinc sparks
224 are not elucidated. In this study, we have examined the role of the zinc
225 transporters ZIP6 and ZIP10 using conditionally gene deficient mice, and queries
226 their contribution to the zinc sparks of fertilization.

227 First, we confirmed the expression of zinc transporter in mouse oocytes.
228 Our results are consistent with previous studies (Kong et al., 2014; Chen et al.,

229 2023). ZIPs, including ZIP6 and ZIP10, are transmembrane proteins (Eide, 2004;
230 Kambe et al., 2004; Lu and Fu, 2007; Schmitt-Ulms et al., 2009). In primordial
231 follicles, the ooplasm staining of ZIP10 we anticipate corresponds to ooplasmic
232 vesicular sites. ZIP10 expression shifted to the plasma membrane in primary and
233 antral follicle phase. A similar localization shift of ZIP10 to the oocyte surface was
234 reported during oocyte maturation, which is much later than reported here by.
235 Furthermore, in that study, ZIP10 was detected in the nuclear/nucleolar positions
236 of oocytes of all follicular stages (Chen et al., 2023), which we did not observe.
237 On the other hand, ZIP6 was expressed at the nuclear/nucleolar regions and in
238 granulosa cells. This localization of ZIP6 was consistent with that in a previous
239 study (Che et al., 2023). However, our results failed to notice that ZIP6 shifts to
240 the at plasma membrane in antral follicle oocytes (Kong et al., 2014; Chen et al.,
241 2023). The results indicate that ZIP6 may be fulfilling a distinct function within the
242 oocytes compared to ZIP10.

243 To assess the role of these transporters in mice, we generated oocyte-
244 specific *Zip6 or Zip10* knockout mice (Fig. S1; *Zip6*$^{d/d}$ and *Zip10*$^{d/d}$, respectively).
245 Previous reports noted that the disruption of these transporters using specific
246 morpholinos or incubation in function-blocking antibodies induced the change of
247 intracellular labile zinc quota into mice oocytes (Kong et al., 2014). The amount
248 of labile zinc ions in those mouse oocytes was measured using Fluozin-3AM, zinc
249 indicator. The amount of labile zinc ions in *Zip10*$^{d/d}$ oocytes was significantly lower
250 than in the *Zip10*$^{f/f}$ (Fig. 2D). We failed to observe any effect on zinc levels of in
251 *Zip6*$^{d/d}$ oocytes (Fig. S2B). The results indicate that ZIP10 is mostly responsible
252 for the uptake of zinc ions in mouse oocytes.

253 Zinc insufficient GV oocytes do not maintain the meiotic arrest at PI (Kong
254 et al., 2012). This is suggested to happen by premature activation of the MOS-
255 MAPK pathway in the presence of low zinc (Kong et al., 2012). In addition, low
256 ooplasmic zinc accelerates meiotic progression that contributes to the extrusion
257 of large polar bodies (Bernhardt et al., 2011). The early mitotic inhibitor 2 (EMI2),
258 a zinc-binding APC/C proteasome inhibitor, is also an essential component of the
259 cytoplasmic factor (CSF) that initiates entry into MII phase. EMI2 is a zinc binding
260 protein, and when zinc is reduced, the activity of the APC/C proteasome is

261 stimulated, increasing the degradation of CCNB1, reduced MPF activity leading
262 to early release of meiosis arrest (Bernhardt et al., 2011; Bernhardt et al., 2012;
263 Suzuki et al., 2010; Shoji et al., 2014; Ohe et al., 2010). Previous studies reported
264 that targeted disruption of *Zip10* using morpholino injections and function-
265 inhibiting antibodies during meiotic maturation perturbed meiosis progression and
266 resulted in cell cycle arrest at the telophase I-like state (Kong et al., 2014). Based
267 on these findings we hypothesized that the reduced state of labile zinc ions in
268 *Zip10*$^{d/d}$ mouse oocytes may resemble the state of zinc-deficient oocytes. We
269 investigated the maturation progression and spindle organization in oocyte
270 matured in vitro from the GV to MII stage. We failed to observe any differences
271 (Fig. 2A, B and C). We also did not observed abnormalities in oocytes from *Zip6*$^{f/f}$
272 mice (Fig. S2A; $p > 0.05$). We speculate that the disparate outcomes observed in
273 previous studies may be attributed to the presence of trace amounts of labile zinc
274 ions in media or in the oocytes.

275 Surprisingly, the amount of labile zinc ions in *Zip10*$^{d/d}$ 2PN zygote was
276 higher than in *Zip10*$^{f/f}$ and despite some differences in fluorescence intensity
277 between *Zip10*$^{d/d}$ GV, MII and 2PN zygote, the labile zinc concentrations were
278 not significantly different between these groups (Fig. 2D). Therefore, we
279 monitored zinc sparks and calcium oscillations in the *Zip10*-KO oocytes. Several
280 studies reported the important of IP_3Rs in mammalian oocytes (Fissore et al.,
281 1999; Parrington et al., 1998), which is essential for egg activation because its
282 inhibition precludes Ca^{2+} oscillations (Miyazaki and Ito, 2006; Miyazaki et al.,
283 1992; Xu et al., 2003). It has been reported that a putative Zinc-finger motif in a
284 helical linker (LNK) domain near the C-terminus of *IP$_3$R1* plays a role in *IP$_3$R1*
285 function (Fan et al., 2015; Paknejad and Hite, 2018). Recently, Akizawa *et al*.,
286 reported that both deficient and excessive zinc ions compromise *IP$_3$R1* sensitivity,
287 diminishing and terminating calcium oscillations (Akizawa et al., 2023). Our
288 results showed that a single zinc spark occurs immediately after first calcium rise
289 of oscillations in *Zip10*$^{f/f}$ oocytes, as reported by Kim *et al* (Kim et al., 2011) (Fig.
290 3A), and similar results are obtained in *Zip6*$^{d/d}$ and *Zip6*$^{f/f}$ mouse oocytes (Fig.
291 S3). However, in *Zip10*$^{d/d}$ oocytes, despite the presence calcium elevations, zinc
292 sparks failed to occur. Similarly, *Zip10*$^{d/d}$ oocytes activated with ionomycin

293 (artificial oocyte activation) did not show a zinc spark (Fig. 3B). In this study,
294 calcium oscillations occurred in oocytes with low zinc state. In addition, there was
295 no difference in the amplitude frequency of calcium ions in oocytes of both groups
296 within the observation time. Akizawa *et al*., produced zinc deficiency state with
297 TPEN, a strong chelator of intracellular labile zinc ions (Akizawa et al., 2023). On
298 the other hand, we did not completely remove intracellular labile zinc ions from
299 mouse oocytes. We speculate that zinc ions existed in *Zip10*$^{d/d}$ mouse oocytes
300 induce Ca^{2+} release without compromising *IP*$_3$*R1* sensitivity. However, this study
301 demonstrated that the accumulation of intracellular zinc ions mediated by ZIP10
302 is essential for inducing zinc sparks in mouse oocytes.

303 The total cellular zinc ions content required for meiosis in the oocyte
304 substantially increases (a 50% increase) from the prophase I arrest to the arrest
305 at metaphase of meiosis II (Kim et al., 2010; Bernhardt et al., 2011). The zinc is
306 stored in undefined cortical granules, and an average of 10^6 zinc atoms are
307 released from these vesicles at the time of fertilization (exocytosis) (Kim et al.,
308 2011; Que et al., 2015; Kong et al., 2014; Que et al., 2019; Jo et al., 2019; Lee
309 et al., 2020). There are several possibilities that might explain why *Zip10*
310 conditional KO mice have low zinc sparks. The most logical is that these oocytes
311 experience reduced zinc loading of cortical of zinc vesicles, leading to the
312 absence of sparks. Our results suggest that in oocytes, zinc sparks and
313 exocytosis require adequate concentrations of labile zinc ions in the cortical
314 secretory vesicles, which is not accomplished when ZIP10 is not present.

315 Zinc sparks have been reported to contribute to the rapid and permanent
316 block mechanisms to prevent polyspermy. The former is achieved by zinc in the
317 extracellular milieu decelerating the forward motility of sperm (Tokuhiro and Dean,
318 2018). Secondly, the release of labile pools of zinc at the same time that the zinc
319 metalloendopeptidase ovastacin is released with the cortical granules (Tokuhiro
320 and Dean, 2018; Burkart et al., 2012; Schmitz et al., 2021), cause ZP2 protein
321 cleavage inducing a complete, although belated block to polyspermy (Que et al.,
322 2017; Aonuma et al., 1981; Tokuhiro and Dean, 2018). However, the
323 physiological significance of the zinc sparks' contributions to polyspermy have
324 not been thoroughly tested, and *Zip10*$^{d/d}$ mice, which are almost devoid of them,

325 offer a great model. Our results showing normal rates of monospermic fertilization
326 in *Zip10*$^{d/d}$ *oocyte* suggest that contributions of Zinc to polyspermy control is
327 negligible (Fig. 4A). Our results also show that the ovastacin undergoes normal
328 release in *Zip10*$^{f/f}$ oocytes after fertilization (Fig. 4E and 4D), confirming previous
329 studies of a minor role of the ZP2 to polyspermy. We observed the disappearance
330 of JUNO after fertilization (Bianchi et al., 2014) *Zip10*$^{d/d}$*,* suggesting that gamete
331 fusion took place (Fig. 4F). Together, these results support the view that zinc
332 spark is not directly involved in the polyspermy rejection mechanism.

333 Interestingly, there were no differences in the rates of fertilization
334 (pronucleus formation), but development to the blastocyst stage was significantly
335 reduced in *Zip10*-null embryos (Fig. 4B). Most of the embryos were arrested at
336 the 2-cell stage and not developed beyond the 4-cell stage. Zinc insufficiency
337 caused altered chromatin structure in the nuclei of blastomeres that displayed
338 decreased global transcription, causing arrest in embryonic development (Kong
339 et al., 2015). The abnormal zinc homeostasis, particularly during the one-cell
340 stage, inhibits the activation of the embryonic genome that occurs around the
341 two-cell stage in mice due to reduce the translational capacity through the
342 inhibition of ribosomal RNA synthesis by RNA polymerase I (Chanfreau, 2013;
343 Garner et al., 2021). Our results also show that *Zip10*$^{d/d}$ blastocysts had
344 significantly lower cell numbers compared to the blastocysts from *Zip10*$^{f/f}$ mice
345 (Fig. 4C). Our results suggest that Zip10$^{d/d}$ mice oocytes can be fertilizable, but
346 their developmental potential is decreased. The lack of ZIP10-mediated zinc
347 influx during the folliculogenesis of *Zip10*$^{d/d}$ may compromise gene expression
348 during these early stages of oocyte development. *Zip10*$^{d/d}$ mouse oocytes thus
349 may have compromised developmental potential from the outset. Future studies
350 should assess the transcriptomic or proteomic profile of *Zip10*$^{d/d}$ mouse oocytes.

351 In conclusion, we elucidated that ZIP10 is required for zinc ion uptake into
352 oocytes and the intracellular zinc ions regulated by ZIP10 was important for zinc
353 sparks and progression of embryonic development. However, the role of ZIP6
354 remained uncertain. Additionally, the absence of mechanistic insight for zinc
355 spark and the inability to distinguish between the developmental and fertilization
356 stage roles of ZIP10 remain unresolved. These challenges necessitate further

357 investigation. Currently, the many infertility patients exist in the world (the survey
358 of WHO). It is reported that approximately half of the adult females are deficient
359 in zinc in their serum (Prasad, 1996; Yokokawa et al., 2020). Zinc has been
360 reported to play essential roles in many physiological functions including
361 reproductive functions (Suzuki, M., et al, 2021, MacDonald RS, 2000, Jackson
362 KA, et al, 2008, Bernhardt ML, et al, 2012, Suzuki, T., et al, 2010, Ohe M, et al,
363 2010). The findings will help elucidate the role of zinc homeostasis in the fields of
364 fertilization/embryogenesis. Furthermore, the development of zinc-focused
365 assisted reproductive technologies and fertilization/embryogenesis media could
366 contribute to improve the developmental potential of oocytes and embryos in
367 other mammalian species.
368

369 **Materials and Methods**

370 All chemicals and reagents were purchased from Sigma-Aldrich (St. Louis, MO,
371 USA) unless otherwise stated.
372

373 **Animals**

374 Animals were housed in the barrier facility at Azabu University. The
375 deletion of the ZIP10 gene in the whole body is known to result in embryonic
376 lethality (He et al., 2023). The conditional knockout mice were generated by Cre-
377 loxP system. The following mouse strains were used: *Zip10*$^{flox/flox}$ (*Zip10*$^{f/f}$) mouse
378 <B6;129-Slc39a10 <tm1.1Tfk>> (RBRC06221) (Hojyo et al., 2014; Miyai et al.,
379 2014; Bin et al., 2017) was provided by the RIKEN BRC through the National
380 BioResource Project of the MEXT/AMED, Japan. *Zip6*$^{flox/flox}$ (*Zip6*$^{f/f}$) mouse
381 <B6;129-Slc39a6> was generated by AdAMS. *Gdf9*$^{Cre/+}$ mice <Stock Tg (GDF9-
382 iCre) 5092Coo/J, Stock No: 011062> were delivered from Jackson Laboratory
383 (Lan Z, et al, 2004). Crlj: C57BL/6J female mice (6-8 weeks old) and Crlj:
384 C57BL/6J male mice (8-12 weeks old) were purchased from Charles River
385 Laboratories Japan (Yokohama, Japan). The mice were housed under controlled
386 lighting conditions (daily light period, 0600-1800 h). The study was approved by
387 the Animal Experimentation Committees of Azabu University and were performed
388 in accordance with the committees' guidelines (200318-13 and 230309-1).

389 Oocyte-specific gene knockout (*Zip10*$^{f/f}$, *Gdf9*$^{Cre/+}$; *Zip10*$^{d/d}$) mice were generated
390 by crossing *Gdf9*$^{Cre/+}$ male mice with *Zip10*$^{f/f}$ female mice (Fig. S1A-E). Similarly,
391 *Zip6*$^{d/d}$ mice were generated (Fig. S1A-E).
392
393 **In situ hybridization (ISH)**
394 ISH was performed as previously described with some modifications
395 (Namiki et al., 2023). Briefly, fixed ovaries were paraffin-embedded and paraffin
396 sections (6 μm) were mounted on MAS-coated slides (Matsunami Glass
397 Industries, Osaka, Japan) under RNase-free conditions. Sense or antisense
398 digoxigenin (DIG)-labeled RNA probes for *Slc39a10* (*Zip10*) were purchased
399 from Genostaff. The sections were deparaffinized, rehydrated, and post-fixed in
400 10% neutral buffered formalin (NBF) for 30 min at 37°C, followed by the treatment
401 with 0.2% hydrogen chloride and 5 μg/ml proteinase K (FUJIFILM Wako Pure
402 Chemical, Osaka, Japan) for 10 min at 37°C, respectively. Hybridization was
403 performed with DIG-labeled probes (250 ng/ml) in a humidified chamber at 60°C
404 overnight. The slides were washed after hybridization, then treated with blocking
405 reagent (Genostaff) for 15 min and alkaline phosphatase-conjugated anti-DIG
406 antibody (1:2,000; Roche Diagnostics, Basel, Switzerland) for 1 h at room
407 temperature. The signals were detected by 4-nitro-blue tetrazolium/5-bromo-4-
408 chloro-3-indolyl phosphate (NBT/BCIP, Roche Diagnostics) in a humidified
409 container for 12 h at 4°C. The sections were counterstained with Kernechtrot
410 solution (Muto Pure Chemicals, Tokyo, Japan). Signals detected by the sense
411 probe were used as a control for background levels.
412
413 **Immunofluorescent staining (IF) for ovary**
414 IF was performed as previously described with some modifications
415 (Namiki et al., 2023). Fixed ovaries were paraffin-embedded and the sections (6
416 μm) were deparaffinized, hydrated and conducted for antigen retrieval by
417 autoclaving in 10 mM sodium citrate buffer (pH = 6.0) for 5 min. The sections
418 were further incubated on ice for 30 min. After blocking with Bloking One Histo
419 (06349-64, NACALAI TESQUE Inc, Kyoto, Japan) for 1 h, the slides were
420 incubated with primary antibody for Rabbit anti-mouse-Zip10 (1:200; (Miyai et al.,

421 2014)), Rabbit anti-SLC39A6 (1:200, HPA042377, Sigma), Rabbit anti-Foxl2
422 (1:300; (Cocquet et al., 2002; Polanco et al., 2010)), Rat anti-ZP2 (1:100, sc-
423 32752, Santa Crus Biotechnology, Dallas, Texas, USA) in Can Get Signal
424 immunostain (TOYOBO, Tokyo, Japan) overnight at 4°C. The slides were
425 incubated with Alexa Fluor 488 donkey anti-rabbit IgG (H+L), Alexa Fluor 594
426 donkey anti-rabbit IgG (H+L) or Alexa Fluor 488 donkey anti-rat IgG (H+L)
427 conjugated secondary antibodies (Jackson Immuno Research Laboratories,
428 West Grove, PA, USA) diluted 1:500 in Can Get Signal immunostain (TOYOBO)
429 for 1 h, and mounted with ProLong Glass Antifade Mountant with NucBlue Stain
430 (P36981, Thermo Fisher Scientific, Waltham, MA, USA). Micrographs were
431 captured by BZ-X700 microscopy (Keyence, Osaka, Japan).
432
433 **Oocyte preparation**
434 Germinal vesicle (GV) oocytes were collected in the manner described in
435 our previous study (Ito et al., 2008) with some modifications. Ovaries were
436 collected from female mice 48 h after intraperitoneally injection with 5 IU equine
437 chorionic gonadotropin (eCG) (PMS; Nippon Zenyaku Kogyo, Fukushima, Japan).
438 They were placed in a 35 mm culture dish containing MEMα (no nucleosides,
439 powder; Gibco/Thermo Fisher Scientific, Tokyo, Japan) medium with 26 mM
440 $NaHCO_3$, 75 mg/l penicillin, 50 mg/l streptomycin sulfate, 5% (v/v) heat-treated
441 fetal calf serum (FCS), and 10 ng/ml epidermal growth factor (EGF). Cumulus-
442 oocyte complexes (COCs) were released from the antral follicles by gentle
443 puncturing with a needle.
444 To obtain metaphase II (MII) oocytes, the mice were intraperitoneally
445 injected with 5 IU eCG followed by injection with 5 IU human chorionic
446 gonadotropin (hCG) (Gonatropin; ASKA Pharmaceutical, Tokyo, Japan) at 48 h
447 later. COCs were collected from the oviductal ampulla 14-16 h after hCG injection.
448 These oocytes were used in the following experiments.
449
450 **Count of ovulated oocytes**
451 COCs-MII were obtained by superovulation treatment. The cumulus cells
452 were removed from the COCs-MII with hyaluronidase (1 mg/ml) and gentle

453 pipetting. All collected oocytes were counted and calculated as the number of
454 ovulations.
455
456 **In vitro maturation (IVM) of GV oocytes**
457 IVM were conducted in the manner described in our previous study
458 (Kamoshita et al., 2021) with some modifications. Ovaries were placed in a 35
459 mm culture dish containing MEMα medium with 26 mM $NaHCO_3$, 75 mg/l
460 penicillin, 50 mg/l streptomycin sulfate, 5% (v/v) FCS, and 10 ng/ml EGF. COCs-
461 GV were released from the antral follicles by gentle puncturing with a needle. The
462 COCs-GV were washed 3 times and cultured in 500 µl of same medium in 4-well
463 dish at 37°C in an atmosphere of 5% CO_2 in air for 10, 12 and 14 h. After the
464 culture, cumulus cells were removed from the COCs with hyaluronidase (1 mg/ml)
465 and gentle pipetting. The extrusion of 1st polar body was evaluated at each time.
466
467 **IF for oocytes/preimplantation embryos**
468 The α-tubulin and JUNO (PE anti-mouse FR4) were performed with some
469 modification of the methods of Inoue *et al* (Inoue et al., 2017). The oocytes or
470 embryos were fixed in 4% PFA for 30 min at room temperature, washed in PBS
471 containing 1% polyvinyl alcohol (PBS/PVA). They were permeabilized by
472 treatment of 0.5% Triton X-100 for 15 min and washed 2 times in 1%
473 BSA/PBS/PVA followed by blocked for 20 min in same medium. They were
474 incubated for overnight at 4° with primary antibodies to rabbit anti-α-tubulin
475 (1:200; 11H10, cell Signaling Technology) or rat anti-mouse FR4 (JUNO; 1:250;
476 12A5 BioLegend), wash 3 times in 1% BSA/PBS/PVA. Primary antibodies were
477 detected using Alexa Fluor 488 donkey anti-rabbit IgG (H+L) (1:250) or Alexa
478 Fluor 488 donkey anti-rat IgG (H+L) (1:250) for 1 h at room temperature. After
479 staining, all samples mounted in VECTASHIELD Mounting Medium with DAPI (H-
480 1200; Vector Laboratories, California, USA), imaged using BZ-X700 microscopy
481 (Keyence, Osaka, Japan).
482 The ovastacin staining was performed with some modifications of the
483 methods of Burkart *et al* (Burkart et al., 2012). oocytes or embryos were fixed in

484 4% PFA for overnight at 4 °C, washed in PBS containing 0.3%
485 polyvinylpyrrolidone (PVP), and then blocked in 0.3% BSA/0.1 M glycine (three
486 times for 10 min) followed by permeabilization in 0.2% Triton X-100 for 15 min
487 (Baibakov et al., 2007). Samples were then incubated for overnight at 4°C with
488 Rabbit polyclonal anti-ovastacin (Burkart et al., 2012), 1:200, gifted antibody),
489 washed with 0.3% PVP/0.1% Tween (three times for 10 min), and incubated for
490 1 h at room temperature with Alexa Fluor 488 anti-rabbit secondary antibody
491 (1:500) followed by staining and mounting with VECTASHIELD Mounting Medium
492 with DAPI. Samples were imaged using TCS SP5 II confocal microscope (Leica
493 Microsystems, Wetzlar, Germany).
494
495 **In vitro fertilization (IVF)**
496 IVF and sperm collection were conducted with some modification of the
497 method described in our previous study (Kageyama et al., 2023). In brief,
498 ovulated COCs-MII were preincubated for 1 h in 80 μl human tubal fluid (HTF)
499 droplets supplemented with 1.25 mM reduced glutathione (GSH). Frozen-thawed
500 sperm suspensions were suspended in 200 μl preincubation medium (HTF
501 containing 0.4 mM methyl-β-cyclodextrin) and 0.1 mg/ml PVA, but without bovine
502 serum albumin, and were incubated at 37 °C under 5% CO_2 in humidified air for
503 1 h. At the time of insemination, preincubated spermatozoa were transferred into
504 the droplets with oocytes at final concentrations of 2.0×10^6 sperm/ml. After 6 h,
505 oocytes were separated from spermatozoa and cumulus cells using a fine glass
506 pipette and transferred into 50 μl KSOMaa medium. They were cultured at 37 °C
507 under 5% CO_2 in humidified air for approximately 24-96 h. The embryos were
508 observed at 24, 48, 72, and 96h after IVF, and the number of 2cell, 4-8cell, morula,
509 and blastocyst stage embryos were counted, respectively. The oocytes used for
510 IVF were calculated as the parameter for the fertilization rate and the rate of
511 embryo development. After IVF at 96 h, the blastocysts were fixed in 4% PFA for
512 30 min at room temperature. Following three times washed in PBS/PVA for 30
513 min each. Nuclear DNA was stained and mounted in VECTASHIELD Mounting
514 Medium with DAPI. Cell numbers were determined by visually inspecting nuclei
515 stained with DAPI using an inverted fluorescence microscope.

516

517 **Zinc measurements**

518 FluoZin-3AM staining was conducted using the method described in our
519 previous study (Kageyama et al., 2022). The obtained GV oocytes, cumulus cells
520 were removed from the COCs with gentle pipetting. The obtained MII oocytes,
521 cumulus cells were removed from the COCs with hyaluronidase (1 mg/ml) and
522 gentle pipetting. Oocytes with a polar body were defined as MII. After IVF for 6h,
523 two pronucleus stage embryos (2PN) were collected. GV, MII and 2PN were
524 loaded in 50 μl medium that was suitable for each stage containing the amyl ester
525 of the membrane permeant zinc-specific fluorophore, FluoZin-3AM (2 μM;
526 F24195, Thermo Fisher Scientific, excitation 494 nm/emission 516 nm) for 1 h in
527 humidified CO_2 [5% (v/v) in air] at 37 ºC followed by washing three times in
528 medium and then observation with TCS SP5 II confocal microscope. FluoZin-3
529 has been extensively characterized for measurements of free intracellular zinc in
530 live cells using microscopy and has an affinity constant (Kd) for zinc of 15 nM
531 (Gee et al., 2002a; Gee et al., 2002b). Our previous study showed MII oocytes
532 were treated with FluoZin-3 AM for 60 min, the change of fluorescence was
533 confirmed in the cytoplasm of the oocytes and embryos, suggesting this treatment
534 duration with FluoZin-3 AM is suitable for detection of zinc ions in oocytes and
535 embryos(Kageyama et al., 2022). The pixel intensity per unit area after
536 background subtraction was determined in GV, MII and 2PN within the circle
537 (white circle) and ImageJ image processing software.

538

539 **Measurement of Ca^{2+} and Zinc spark during fertilization**

540 Fresh or frozen-thawed sperm suspension were suspended in 200 μl
541 preincubation medium. The 1 μl (fresh) or 20 μl (frozen-thawed) sperm
542 suspension were placed in 40-80 μl HTF drop in pre-insemination dish about 20
543 min before insemination. The zona pellucida were punctured by piezo-electric
544 pulses applied to four locations with a 15 μm injection needle. The treated MII
545 oocytes were cultured in CZB containing CalbryteTM 590 AM (10 μM, #20700,
546 AAT Bioquest, CA, USA, excitation 581 nm/emission 593 nm) for 10 min in
547 humidified CO_2 [5% (v/v) in air] at 37 °C. While the oocytes are incubated for 10

548 min, make a drop of 10 µl of PVA(-), Ca(-) Hepes-CZB (H-CZB) and pull out 7 µl
549 of medium from drop with pipette man in the insemination dish. After 10 min, the
550 oocytes are washed and transferred to insemination dish and the oocytes are
551 attached to the dish. After attachment, an HTF containing 7 µl of BSA and a
552 membrane-impermeable zinc-specific fluorophore, FluoZin-3 (20 µM, F24194,
553 Thermo Fisher Scientific, excitation 494 nm/emission 516 nm), is added to the 3
554 µl drop containing the oocytes gently using a capillary. The about 1 µl sperm were
555 sucked from the pre-insemination drop with the capillary under a
556 stereomicroscope and place into the drop containing the oocytes, to start imaging.
557 In case ionomycin treatment, after calcium labeling, MII were allowed to settle in
558 45 µl PVA(-), Ca(-) H-CZB containing FluoZin-3 medium drop on dish, to start
559 imaging. The 5 µl ionomycin (5 µM; #407950) were added to MII at 2 min after
560 imaging start. Imaging was performed on confocal microscope using 488 nm
561 (Zn^{2+}) and 555 nm (Ca^{2+}) excitation (Nikon solutions, Tokyo, Japan) for max 50
562 min every 4 seconds. Imaging analysis was performed by defining regions of
563 interest (ROIs) and measuring fluorescence intensity over time using NIS-
564 Elements (Nikon). The intracellular ROIs were drawn as the entire interior area
565 of the cell. The extracellular ROIs were defined as a ring around the perimeter of
566 cell. The ring thickness was conserved for all data analyses.
567
568 **Western blotting**
569 Western blotting was carried out as described (Ito et al., 2010) with some
570 modifications. Thirty MII oocytes or 2PN embryos were lysed in Laemmli sample
571 buffer (Bio-Rad Laboratories, Tokyo, Japan) with 5% 2-mercaptoethanol.
572 Samples were separated on 8% Bis-Tris gels by SDS-PAGE and transferred to
573 PVDF membranes (Bio-Rad). The PVDF membranes were blocked in 10% skim
574 milk (FUJIFILM Wako) in Tris-buffered saline (TBS) with 0.1% Tween-20
575 (Yoneyama yakuhin kogyo, Osaka, Japan) and probed with primary antibody to
576 Rabbit anti-mouse-Zip10 (1:1,000; (Miyai et al., 2014)), Rabbit anti-SLC39A6
577 (1:1,000, HPA042377), rat anti-ZP2 (1:1,000) or monoclonal mouse anti-β-actin
578 (1:5,000; A5316, Sigma-Aldrich) for overnight at 4°C. The membranes were
579 incubated with secondary antibody; HRP-conjugated anti-rabbit IgG (1:5,000;

580 Cell Signaling Technology, Danvers, MA, USA), HRP-conjugated anti-rat IgG
581 (1:5000; Cell Signaling Technology) or HRP-conjugated anti-mouse IgG (1:5,000;
582 Cell Signaling Technology) for 1 h at room temperature. After washing of the
583 membranes, immunoreactive proteins were visualized using ECL™ Western
584 Blotting Analysis System (Cytiva Global Life Sciences Technologies, Tokyo,
585 Japan), according to the manufacture's recommendation. The membranes were
586 exposed by ImageQuant LAS 4000. After exposure, the membranes were
587 incubated for 30 min at 50 °C in the stripping buffer including 1.5 M Tris-HCl (pH
588 6.8), 10% SDS, 2-mercaptoethanol followed by extensive washing of the
589 membranes. The membranes were probed with primary antibody to mouse anti-
590 β-actin (1:5000; Sigma-Aldrich) for overnight at 4°C. The membranes were
591 incubated with secondary antibody; FRP-conjugated anti-mouse IgG (1:5000;
592 Cell Signaling) for 1 h at room temperature. The same procedure was followed
593 below. The intensities of ZP2 bands were measured by quantitative analysis by
594 densitometry using Image J.
595
596 **Statistical analysis**
597 Values from three or more times were used for evaluation of statistical
598 significance. Statistical analysis was performed using Statcel 3 software (OMS
599 Ltd., Saitama, Japan). The fertility, the total numbers of oocytes collected from
600 each mouse, the percentage of first polar extrusions, the fluorescence intensity
601 of Fluozin-3 AM, the cell count of blastocysts and Quantification of JUNO
602 expression were evaluated statistically by Student's or welch's *t*-test analysis.
603 The rate of fertilization and embryo development was analyzed using chi square
604 tests. The Quantification of ZP2 expression before and after fertilization was
605 analyzed using one-way ANOVA. Values are shown as means ± S.E.M, and
606 significant differences were considered at p values < 0.05.
607
608
609 **Acknowledgments and funding sources**
610 We thank the members of the Laboratory of Animal Reproduction, School of

Veterinary Medicine, Azabu University for technical help. *Zip10*$^{flox/flox}$ (*Zip10*$^{f/f}$) mouse <B6;129-Slc39a10 <tm1.1Tfk>> (RBRC06221) was provided by the RIKEN BRC through the National BioResource Project of the MEXT/AMED, Japan. We also thank Dr. Austin J. Cooney (The University of Texas at Austin, Austin, United States) for providing GDF9-iCre mice. This research was supported by Grants-in-Aid for Scientific Research from the Japan Society for the Promotion of Science (JSPS) (KAKENHI, 21H02384 and 20H05373 to J.I., 22H04268, 24H02601 and 24K23214 to A.K.), JSPS KAKENHI Grant Number JP 15H04584 (AdAMS) to JI, the Sasakawa Scientific Research Grant from The Japan Science Society (2019-4044) to A.K. and Mishima Kaiun Memorial Foundation (A-135) to A.K. This work was supported by JSPS KAKENHI Grant Number JP 22H04922 (AdAMS). This study was also supported by Center for Diversity, Equity & Inclusion, Azabu University (A.K). This research was partially supported by the Center for Human and Animal Symbiosis Science, Azabu University and a research project grant awarded by the Azabu University Research Services Division to J.I.

Author contributions

Conceptualization: A.K., J.I., Data curation: A.K., Methodology: N.O., T.W., A.O., Investigation: A.K., N.O., T.N., Y.K., Resources: M.O., Y.Y., T.F., Visualization: A.K., N.O., T.N., Supervision: A.O., T.F., R.A.F. J.I., N.K., Writing—original draft: A.K., Writing—review & editing: All the authors reviewed and edited the manuscript.

Competing interests

All other authors declare they have no competing interests.

Data and materials availability

All data are available in the main text or the supplementary materials.

References

Akizawa H, Lopes E, Fissore RA. 2023. Zn(2+) is Essential for Ca(2+) Oscillations in Mouse Eggs. *bioRxiv* doi:10.1101/2023.04.13.536745

Allouche-Fitoussi D, Breitbart H. 2020. The Role of Zinc in Male Fertility. *Int.J.Mol.Sci*. **21:**7796. doi: 10.3390/ijms21207796. doi:10.3390/ijms21207796

Aonuma S, Okabe M, Kawaguchi M, Kishi Y. 1981. Zinc effects on mouse spermatozoa and in-vitro fertilization. *J.Reprod.Fertil.* **63:**463–466. doi:10.1530/jrf.0.0630463

Baibakov B, Gauthier L, Talbot P, Rankin TL, Dean J. 2007. Sperm binding to the zona pellucida is not sufficient to induce acrosome exocytosis. *Development* **134:**933–943. doi:10.1242/dev.02752

Bedwal RS, Bahuguna A. 1994. Zinc, copper and selenium in reproduction. *Experientia* **50:**626–640. doi:10.1007/BF01952862

Bernhardt ML, Kim AM, O'Halloran TV, Woodruff TK. 2011. Zinc requirement during meiosis I-meiosis II transition in mouse oocytes is independent of the MOS-MAPK pathway. *Biol.Reprod.* **84:**526–536. doi:10.1095/biolreprod.110.086488

Bernhardt ML, Kong BY, Kim AM, O'Halloran TV, Woodruff TK. 2012. A zinc-dependent mechanism regulates meiotic progression in mammalian oocytes. *Biol.Reprod*. **86:**114. doi:10.1095/biolreprod.111.097253

Bianchi E, Doe B, Goulding D, Wright GJ. 2014. Juno is the egg Izumo receptor and is essential for mammalian fertilization. *Nature* **508:**483–487. doi:10.1038/nature13203

Bin B, Bhin J, Takaishi M, Toyoshima K, Kawamata S, Ito K, Hara T, Watanabe T, Irie T, Takagishi T, Lee S, Jung H, Rho S, Seo J, Choi D, Hwang D, Koseki H, Ohara O, Sano S, Tsuji T, Mishima K, Fukada T. 2017. Requirement of zinc transporter ZIP10 for epidermal development: Implication of the ZIP10-p63 axis in epithelial homeostasis. *Proc.Natl.Acad.Sci.U.S.A.* **114:**12243–12248. doi:10.1073/pnas.1710726114

Burkart AD, Xiong B, Baibakov B, Jimenez-Movilla M, Dean J. 2012. Ovastacin, a cortical granule protease, cleaves ZP2 in the zona pellucida to prevent polyspermy. *J.Cell Biol.* **197:**37–44. doi:10.1083/jcb.201112094

Chanfreau GF. 2013. Zinc'ing down RNA polymerase I. *Transcription* **4:**217–220. doi:10.4161/trns.26594

Chen Y, Chen S, Ok K, Duncan FE, O'Halloran TV, Woodruff TK. 2023. Zinc dynamics regulate early ovarian follicle development. *J.Biol.Chem*. **299:**102731. doi:10.1016/j.jbc.2022.102731

679 Cocquet J, Pailhoux E, Jaubert F, Servel N, Xia X, Pannetier M, De Baere E,
680 Messiaen L, Coti C, Fellous M, Veitia RA. 2002. Evolution and expression of
681 FOXL2. *J.Med.Genet.* **39:**916–921. doi:10.1136/jmg.39.12.916

682 Ducibella T, Schultz RM, Ozil J. 2006. Role of calcium signals in early
683 development. *Semin.Cell Dev.Biol.* **17:**324–332.
684 doi:10.1016/j.semcdb.2006.02.010

685 Duncan FE, Que EL, Zhang N, Feinberg EC, O'Halloran TV, Woodruff TK.
686 2016. The zinc spark is an inorganic signature of human egg activation.
687 *Sci.Rep.* **6:**24737. doi:10.1038/srep24737

688 Eide DJ. 2004. The SLC39 family of metal ion transporters. *Pflugers Arch.*
689 **447:**796–800. doi:10.1007/s00424-003-1074-3

690 Fan G, Baker ML, Wang Z, Baker MR, Sinyagovskiy PA, Chiu W, Ludtke SJ,
691 Serysheva II. 2015. Gating machinery of InsP3R channels revealed by electron
692 cryomicroscopy. *Nature* **527:**336–341. doi:10.1038/nature15249

693 Favier AE. 1992. The role of zinc in reproduction. Hormonal mechanisms.
694 *Biol.Trace Elem.Res.* **32:**363–382. doi:10.1007/BF02784623

695 Fissore RA, Longo FJ, Anderson E, Parys JB, Ducibella T. 1999. Differential
696 distribution of inositol trisphosphate receptor isoforms in mouse oocytes.
697 *Biol.Reprod.* **60:**49–57. doi:10.1095/biolreprod60.1.49

698 Fukada T, Kambe T. 2011. Molecular and genetic features of zinc transporters
699 in physiology and pathogenesis. *Metallomics* **3:**662–674.
700 doi:10.1039/c1mt00011j

701 Garner TB, Hester JM, Carothers A, Diaz FJ. 2021. Role of zinc in female
702 reproduction. *Biol.Reprod*. **104:**976–994. doi:10.1093/biolre/ioab023

703 Gee KR, Zhou ZL, Qian WJ, Kennedy R. 2002a. Detection and imaging of zinc
704 secretion from pancreatic beta-cells using a new fluorescent zinc indicator.
705 *J.Am.Chem.Soc.* **124:**776–778. doi:ja011774y [pii]

706 Gee KR, Zhou ZL, Ton-That D, Sensi SL, Weiss JH. 2002b. Measuring zinc in
707 living cells. A new generation of sensitive and selective fluorescent probes. *Cell*
708 *Calcium* **31:**245–251. doi:10.1016/S0143-4160(02)00053-2

709 He X, Ge C, Xia J, Xia Z, Zhao L, Huang S, Wang R, Pan J, Cheng T, Xu P,
710 Wang F, Min J. 2023. The Zinc Transporter SLC39A10 Plays an Essential Role
711 in Embryonic Hematopoiesis. *Adv.Sci.(Weinh)* **10:**e2205345.
712 doi:10.1002/advs.202205345

713 Hojyo S, Miyai T, Fujishiro H, Kawamura M, Yasuda T, Hijikata A, Bin B, Irie T,
714 Tanaka J, Atsumi T, Murakami M, Nakayama M, Ohara O, Himeno S, Yoshida
715 H, Koseki H, Ikawa T, Mishima K, Fukada T. 2014. Zinc transporter
716 SLC39A10/ZIP10 controls humoral immunity by modulating B-cell receptor
717 signal strength. *Proc.Natl.Acad.Sci.U.S.A.* **111:**11786–11791.
718 doi:10.1073/pnas.1323557111

719 Inoue A, Jiang L, Lu F, Suzuki T, Zhang Y. 2017. Maternal H3K27me3 controls
720 DNA methylation-independent imprinting. *Nature* **547:**419–424.
721 doi:10.1038/nature23262

722 Ito J, Parrington J, Fissore RA. 2011. PLCzeta and its role as a trigger of
723 development in vertebrates. *Mol.Reprod.Dev*. **78:**846–853.
724 doi:10.1002/mrd.21359

725 Ito J, Yoon S, Lee B, Vanderheyden V, Vermassen E, Wojcikiewicz R, Alfandari
726 D, De Smedt H, Parys JB, Fissore RA. 2008. Inositol 1,4,5-trisphosphate
727 receptor 1, a widespread Ca2+ channel, is a novel substrate of polo-like kinase
728 1 in eggs. *Dev.Biol*. **320:**402–413. doi:10.1016/j.ydbio.2008.05.548

729 Ito J, Yoshida T, Kasai Y, Wakai T, Parys JB, Fissore RA, Kashiwazaki N. 2010.
730 Phosphorylation of inositol 1,4,5-triphosphate receptor 1 during in vitro
731 maturation of porcine oocytes. *Anim.Sci.J*. **81:**34–41. doi:10.1111/j.1740-
732 0929.2009.00699.x

733 Jackson KA, Valentine RA, Coneyworth LJ, Mathers JC, Ford D. 2008.
734 Mechanisms of mammalian zinc-regulated gene expression.
735 *Biochem.Soc.Trans*. **36:**1262–1266. doi:10.1042/BST0361262

736 Jo Y, Lee I, Jung S, Kwon J, Kim N, Namgoong S. 2019. Spire localization via
737 zinc finger-containing domain is crucial for the asymmetric division of mouse
738 oocyte. *FASEB J*. **33:**4432–4447. doi:10.1096/fj.201801905R

739 Jones KT. 2005. Mammalian egg activation: from Ca2+ spiking to cell cycle
740 progression. *Reproduction* **130:**813–823. doi:10.1530/rep.1.00710

741 Kageyama A, Terakawa J, Ito J, Kashiwazaki N. 2022. Roles of zinc signaling in
742 mammalian reproduction. *Metallomics Research*. **2**

743 Kageyama A, Suyama A, Kinoshita R, Ito J, Kashiwazaki N. 2022. Dynamic
744 changes of intracellular zinc ion level during maturation, fertilization, activation,
745 and development in mouse oocytes. *Anim.Sci.J*. **93:**e13759.
746 doi:10.1111/asj.13759

747 Kageyama A, Tsuchiya M, Terakawa J, Ito J, Kashiwazaki N. 2023. A combined
748 treatment with progesterone, anti-inhibin serum, and equine chorionic

749 gonadotropin improves number of ovulated oocytes in young C57BL/6J mice.
750 *J.Reprod.Dev*. **69:**223–226. doi:10.1262/jrd.2023-036

751 Kambe T, Yamaguchi-Iwai Y, Sasaki R, Nagao M. 2004. Overview of
752 mammalian zinc transporters. *Cell Mol.Life Sci*. **61:**49–68. doi:10.1007/s00018-
753 003-3148-y

754 Kambe T, Tsuji T, Hashimoto A, Itsumura N. 2015. The Physiological,
755 Biochemical, and Molecular Roles of Zinc Transporters in Zinc Homeostasis
756 and Metabolism. *Physiol.Rev*. **95:**749–784. doi:10.1152/physrev.00035.2014

757 Kamoshita M, Fujiwara K, Ito J, Kashiwazaki N. 2021. Highly successful
758 production of viable mice derived from vitrified germinal vesicle oocytes. *PLoS*
759 *One* **16:**e0248050. doi:10.1371/journal.pone.0248050

760 Kim AM, Bernhardt ML, Kong BY, Ahn RW, Vogt S, Woodruff TK, O'Halloran
761 TV. 2011. Zinc sparks are triggered by fertilization and facilitate cell cycle
762 resumption in mammalian eggs. *ACS Chem.Biol*. **6:**716–723.
763 doi:10.1021/cb200084y

764 Kim AM, Vogt S, O'Halloran TV, Woodruff TK. 2010. Zinc availability regulates
765 exit from meiosis in maturing mammalian oocytes. *Nat.Chem.Biol.* **6:**674–681.
766 doi:10.1038/nchembio.419

767 Kong BY, Duncan FE, Que EL, Kim AM, O'Halloran TV, Woodruff TK. 2014.
768 Maternally-derived zinc transporters ZIP6 and ZIP10 drive the mammalian
769 oocyte-to-egg transition. *Mol.Hum.Reprod*. **20:**1077–1089.
770 doi:10.1093/molehr/gau066

771 Kong BY, Bernhardt ML, Kim AM, O'Halloran TV, Woodruff TK. 2012. Zinc
772 maintains prophase I arrest in mouse oocytes through regulation of the MOS-
773 MAPK pathway. *Biol.Reprod*. **87:**11, 1–12. doi:10.1095/biolreprod.112.099390

774 Kong BY, Duncan FE, Que EL, Xu Y, Vogt S, O'Halloran TV, Woodruff TK.
775 2015. The inorganic anatomy of the mammalian preimplantation embryo and
776 the requirement of zinc during the first mitotic divisions. *Dev.Dyn*. **244:**935–947.
777 doi:10.1002/dvdy.24285

778 Lan Z, Xu X, Cooney AJ. 2004. Differential oocyte-specific expression of Cre
779 recombinase activity in GDF-9-iCre, Zp3cre, and Msx2Cre transgenic mice.
780 *Biol.Reprod*. **71:**1469–1474. doi:10.1095/biolreprod.104.031757

781 Lee HC, Edmonds ME, Duncan FE, O'Halloran TV, Woodruff TK. 2020. Zinc
782 exocytosis is sensitive to myosin light chain kinase inhibition in mouse and
783 human eggs. *Mol.Hum.Reprod*. **26:**228–239. doi:10.1093/molehr/gaaa017

Lu M, Fu D. 2007. Structure of the zinc transporter YiiP. *Science* **317:**1746–1748. doi:10.1126/science.1143748

Lubna S, Ahmad R. 2023. Clinical and biochemical understanding of Zinc interaction during liver diseases: A paradigm shift. *J.Trace Elem.Med.Biol*. **77:**127130. doi:10.1016/j.jtemb.2023.127130

MacDonald RS. 2000. The role of zinc in growth and cell proliferation. *J.Nutr.* **130:**1500S–8S. doi:10.1093/jn/130.5.1500S

Miyai T, Hojyo S, Ikawa T, Kawamura M, Irie T, Ogura H, Hijikata A, Bin B, Yasuda T, Kitamura H, Nakayama M, Ohara O, Yoshida H, Koseki H, Mishima K, Fukada T. 2014. Zinc transporter SLC39A10/ZIP10 facilitates antiapoptotic signaling during early B-cell development. *Proc.Natl.Acad.Sci.U.S.A*. **111:**11780–11785. doi:10.1073/pnas.1323549111

Miyazaki S, Yuzaki M, Nakada K, Shirakawa H, Nakanishi S, Nakade S, Mikoshiba K. 1992. Block of Ca2+ wave and Ca2+ oscillation by antibody to the inositol 1,4,5-trisphosphate receptor in fertilized hamster eggs. *Science* **257:**251–255. doi:10.1126/science.1321497

Miyazaki S, Ito M. 2006. Calcium signals for egg activation in mammals. *J.Pharmacol.Sci*. **100:**545–552. doi:10.1254/jphs.cpj06003x

Namiki T, Terakawa J, Karakama H, Noguchi M, Murakami H, Hasegawa Y, Ohara O, Daikoku T, Ito J, Kashiwazaki N. 2023. Uterine epithelial Gp130 orchestrates hormone response and epithelial remodeling for successful embryo attachment in mice. *Sci.Rep*. **13:**854–y. doi:10.1038/s41598-023-27859-y

Ohe M, Kawamura Y, Ueno H, Inoue D, Kanemori Y, Senoo C, Isoda M, Nakajo N, Sagata N. 2010. Emi2 inhibition of the anaphase-promoting complex/cyclosome absolutely requires Emi2 binding via the C-terminal RL tail. *Mol.Biol.Cell* **21:**905–913. doi:10.1091/mbc.e09-11-0974

Paknejad N, Hite RK. 2018. Structural basis for the regulation of inositol trisphosphate receptors by Ca(2+) and IP(3). *Nat.Struct.Mol.Biol.* **25:**660–668. doi:10.1038/s41594-018-0089-6

Parrington J, Brind S, De Smedt H, Gangeswaran R, Lai FA, Wojcikiewicz R, Carroll J. 1998. Expression of inositol 1,4,5-trisphosphate receptors in mouse oocytes and early embryos: the type I isoform is upregulated in oocytes and downregulated after fertilization. *Dev.Biol.* **203:**451–461. doi:10.1006/dbio.1998.9071

Pascua AM, Nikoloff N, Carranza AC, Anchordoquy JP, Quintana S, Barbisan G, Diaz S, Anchordoquy JM, Furnus CC. 2020. Reproductive hormones

821 influence zinc homeostasis in the bovine cumulus-oocyte complex: Impact on
822 intracellular zinc concentration and transporters gene expression.
823 *Theriogenology* **146:**48–57. doi:10.1016/j.theriogenology.2020.01.054

824 Polanco JC, Wilhelm D, Davidson T, Knight D, Koopman P. 2010. Sox10 gain-
825 of-function causes XX sex reversal in mice: implications for human 22q-linked
826 disorders of sex development. *Hum.Mol.Genet.* **19:**506–516.
827 doi:10.1093/hmg/ddp520

828 Prasad AS. 1996. Zinc deficiency in women, infants and children.
829 *J.Am.Coll.Nutr*. **15:**113–120. doi:10.1080/07315724.1996.10718575

830 Que EL, Bleher R, Duncan FE, Kong BY, Gleber SC, Vogt S, Chen S, Garwin
831 SA, Bayer AR, Dravid VP, Woodruff TK, O'Halloran TV. 2015. Quantitative
832 mapping of zinc fluxes in the mammalian egg reveals the origin of fertilization-
833 induced zinc sparks. *Nat.Chem*. **7:**130–139. doi:10.1038/nchem.2133

834 Que EL, Duncan FE, Bayer AR, Philips SJ, Roth EW, Bleher R, Gleber SC,
835 Vogt S, Woodruff TK, O'Halloran TV. 2017. Zinc sparks induce physiochemical
836 changes in the egg zona pellucida that prevent polyspermy. *Integr.Biol.(Camb)*
837 **9:**135–144. doi:10.1039/c6ib00212a

838 Que EL, Duncan FE, Lee HC, Hornick JE, Vogt S, Fissore RA, O'Halloran TV,
839 Woodruff TK. 2019. Bovine eggs release zinc in response to parthenogenetic
840 and sperm-induced egg activation. *Theriogenology* **127:**41–48.
841 doi:10.1016/j.theriogenology.2018.12.031

842 Saunders CM, Larman MG, Parrington J, Cox LJ, Royse J, Blayney LM, Swann
843 K, Lai FA. 2002. PLC zeta: a sperm-specific trigger of Ca(2+) oscillations in
844 eggs and embryo development. *Development* **129:**3533–3544.
845 doi:10.1242/dev.129.15.3533

846 Schmitt-Ulms G, Ehsani S, Watts JC, Westaway D, Wille H. 2009. Evolutionary
847 descent of prion genes from the ZIP family of metal ion transporters. *PLoS One*
848 **4:**e7208. doi:10.1371/journal.pone.0007208

849 Schmitz C, Sadr SZ, Korschgen H, Kuske M, Schoen J, Stocker W, Jahnen-
850 Dechent W, Floehr J. 2021. The E-modulus of the oocyte is a non-destructive
851 measure of zona pellucida hardening. *Reproduction* **162:**259–266.
852 doi:10.1530/REP-21-0122

853 Seeler JF, Sharma A, Zaluzec NJ, Bleher R, Lai B, Schultz EG, Hoffman BM,
854 LaBonne C, Woodruff TK, O'Halloran TV. 2021. Metal ion fluxes controlling
855 amphibian fertilization. *Nat.Chem*. **13:**683–691. doi:10.1038/s41557-021-00705-
856 2

857 Shoji S, Muto Y, Ikeda M, He F, Tsuda K, Ohsawa N, Akasaka R, Terada T,
858 Wakiyama M, Shirouzu M, Yokoyama S. 2014. The zinc-binding region (ZBR)
859 fragment of Emi2 can inhibit APC/C by targeting its association with the
860 coactivator Cdc20 and UBE2C-mediated ubiquitylation. *FEBS Open Bio* **4:**689–
861 703. doi:10.1016/j.fob.2014.06.010

862 Sugita H, Takarabe S, Kageyama A, Kawata Y, Ito J. 2024. Molecular
863 Mechanism of Oocyte Activation in Mammals: Past, Present, and Future
864 Directions. *Biomolecules* **14:**359. doi: 10.3390/biom14030359.
865 doi:10.3390/biom14030359

866 Suzuki M, Suzuki T, Watanabe M, Hatakeyama S, Kimura S, Nakazono A,
867 Honma A, Nakamaru Y, Vreugde S, Homma A. 2021. Role of intracellular zinc
868 in molecular and cellular function in allergic inflammatory diseases. *Allergol.Int*.
869 **70:**190–200. doi:10.1016/j.alit.2020.09.007

870 Suzuki T, Yoshida N, Suzuki E, Okuda E, Perry ACF. 2010. Full-term mouse
871 development by abolishing Zn2+-dependent metaphase II arrest without Ca2+
872 release. Development **137:**2659–2669. doi:10.1242/dev.049791

873 Takagishi T, Hara T, Fukada T. 2017. Recent Advances in the Role of
874 SLC39A/ZIP Zinc Transporters In Vivo. *Int.J.Mol.Sci.* **18:**2708. doi:
875 10.3390/ijms18122708. doi:10.3390/ijms18122708

876 Tian X, Diaz FJ. 2012. Zinc depletion causes multiple defects in ovarian
877 function during the periovulatory period in mice. *Endocrinology* **153:**873–886.
878 doi:10.1210/en.2011-1599

879 Tokuhiro K, Dean J. 2018. Glycan-Independent Gamete Recognition Triggers
880 Egg Zinc Sparks and ZP2 Cleavage to Prevent Polyspermy. *Dev.Cell*. **46:**627–
881 640.e5. doi:10.1016/j.devcel.2018.07.020

882 Xu Z, Kopf GS, Schultz RM. 1994. Involvement of inositol 1,4,5-trisphosphate-
883 mediated Ca2+ release in early and late events of mouse egg activation.
884 *Development* **120:**1851–1859. doi:10.1242/dev.120.7.1851

885 Xu Z, Williams CJ, Kopf GS, Schultz RM. 2003. Maturation-associated increase
886 in IP3 receptor type 1: role in conferring increased IP3 sensitivity and Ca2+
887 oscillatory behavior in mouse eggs. *Dev.Biol*. **254:**163–171. doi:10.1016/s0012-
888 1606(02)00049-0

889 Yokokawa H, Fukuda H, Saita M, Miyagami T, Takahashi Y, Hisaoka T, Naito T.
890 2020. Serum zinc concentrations and characteristics of zinc deficiency/marginal
891 deficiency among Japanese subjects. *J.Gen.Fam.Med*. **21:**248–255.
892 doi:10.1002/jgf2.377

Yoon S, Fissore RA. 2007. Release of phospholipase C zetaand [Ca2+]i oscillation-inducing activity during mammalian fertilization. *Reproduction* **134:**695–704. doi:10.1530/REP-07-0259

Figure legends

Fig. 1. Expression of ZIP6 and ZIP10 in mouse ovary. (A) In situ hybridization in the mouse ovary showed ZIP10 expression in oocyte and granulosa cell from primordial, primary, secondary and antral follicle. Arrow indicates primordial follicular oocyte. (**B**) Immunofluorescent staining for ZIP10 (green) in the mouse ovary showed ZIP10 expression in oocyte membrane. Arrow indicates primordial follicular oocyte. (**C**) Immunofluorescent staining for ZIP6 (green) in the mouse ovary showed ZIP6 expression in oocyte nucleus and granulosa cells. Arrow indicates primordial follicular oocyte. (**D**) Immunofluorescent staining showed ZP2 (green; zona pellucida) and FOXL2 (red; granulosa cells) in the mouse ovary. It was observed that ZP2 was not present in the primordial follicle; however, it was present in the primary, secondary and antral follicles. Furthermore, FOXL2 was observed at granulosa cells of all stage follicles. Scale bar: 20 μm (primordial, primary and secondary follicle); 150 μm (antral follicle) (**A-D**).

Fig. 2 Number of collected oocytes and dynamics of labile zinc ion in *Zip10$^{d/d}$* mice. (**A**) The results of average number of oocytes in each group. Data represents the average ± SEM. These experiments were repeated at least thrice. Statistical differences were calculated according to student's *t*-test ($p > 0.05$; no significant difference). (**B**) The percentage of extrusion of first polar body at 10, 12 and 14 h after IVM. These experiments were repeated at least thrice. Statistical differences were calculated according to student's *t*-test ($p > 0.05$; no

923 significant difference). (**C**) The morphology of spindle and chromosome
924 organization in *Zip10*$^{f/f}$ and *Zip10*$^{d/d}$ MII oocytes at 14 h after IVM. Anti–α-tubulin
925 antibody (green) was used to stain the spindles. Chromosomes were stained with
926 DAPI (blue). The scale bar represents 10 μm. (**D**) Comparison with the
927 fluorescence intensity of intracellular labile zinc ion in GV, MII and 2PN. The
928 upper images showed the fluorescence of intracellular labile zinc ion of oocyte or
929 embryo treated with 2 μM FluoZin-3AM for 1h. Representative images are shown.
930 The white dotted circles indicate the positions of oocytes and embryos. Scale
931 bars denote 10 μm. The lower part showed the fluorescence intensity of labile
932 zinc ions in oocytes or embryos. Data represent the average ± SE of the
933 experiments. For each experiment, 10–20 oocytes/embryos were stained and
934 used for the measurement in each stage of the experiment, and these
935 experiments were repeated three times. Statistical differences were calculated
936 according to the welch's *t*-test. Different letters represent significant differences
937 ($p < 0.05$).
938
939 **Fig. 3 Measurement of calcium spike and zinc spark in *Zip10*$^{d/d}$ mice.** (**A**)
940 The representative images of calcium spike and zinc spark after IVF in mouse
941 oocytes. Left side images showed calcium spike. Right side images showed zinc
942 spark. The oocytes increased calcium ion and released zinc ion shortly after
943 fertilization. The white dotted circles indicate the positions of oocytes. Successful
944 fertilization was confirmed by simultaneously monitoring intracellular calcium
945 oscillations with Calbryte 590 AM and excellular zinc ions with FluoZin-3 every 4
946 s. Capacitated frozen-thawed sperm was added to MII at 2 min after imaging start.
947 Orange line showed calcium ion and dark blue line showed zinc ion. Intracellular
948 calcium increases immediately before a zinc spark. Scale bars denote 20 μm. (**B**)
949 The representative images of an MII egg activated with 5 μM ionomycin followed
950 by monitoring of intracellular calcium oscillations with Calbryte 590 AM and
951 extracellular zinc using 20 μM FluoZin-3. The ionomycin was added to MII at 2
952 min after imaging start. Orange line showed calcium ion and dark blue line
953 showed zinc ion. Intracellular calcium increases immediately before a zinc spark.
954 Scale bars denote 20 μm.

955

956 **Fig. 4 Presence of a mechanism to prevent multisperm fertilization in Zip10**
957 **cKO mice.** (**A**) The percentages of oocytes with each number of PN at 6 h after
958 insemination. Yellow region showed other including degeneration, degression
959 and fragmentation. Gray region showed unfertilization, namely MII oocytes.
960 Orange showed 2PN2PB, namely embryo possessed one female and male
961 pronucleous (2PN) and second polar body (2PB). Blue region showed multisperm
962 fertilization (3PN2PB). (**B**) The percentage of fertilized oocytes and
963 developmental embryos. Data represent the average ± SE of the experiments.
964 The embryo development was observed at 6 (2PN) 24 (2 cell), 48 (4-8 cell), 72
965 (Morula), and 96 (Blastocyst) hours after IVF. The oocytes used for IVF were
966 calculated as the parameter for the fertilization rate and the rate of embryo
967 development. These experiments were repeated at least thrice. Statistical
968 differences were calculated according to the chi-square test. Different letters
969 represent significant differences ($p < 0.05$). (**C**) The cell number of blastocyst
970 derived from IVF. Blastocysts were fixed, immunostained, and physically
971 flattened between a slide and coverslip. Photographs represent a single plane of
972 focus. Nuclei are indicated by DAPI staining. The count used inverted
973 fluorescence microscope. These experiments were repeated three times, and
974 each group counted total 46 embryos. Statistical differences were calculated
975 according to the student's *t*-test ($p < 0.05$; significant difference). (**D**) Western blot
976 of oocytes from *Zip10*$^{f/f}$ and *Zip10*$^{d/d}$ mice at 0 or 6 h after insemination using rat
977 anti-ZP2 antibody. Intact ZP2 and the cleaved C-terminal fragment of ZP2
978 measured 120-130 kD and undetected, respectively. Expression level of β-actin
979 serves as a protein loading control and quantified the expression level of ZP2.
980 Molecular mass is indicated at the left. Statistical differences were calculated
981 according to the one-way ANOVA. Different letters represent significant
982 differences ($p < 0.05$). (**E**) MII oocytes and 2PN embryos from *Zip10*$^{f/f}$ and *Zip10*$^{d/d}$
983 mice were imaged by confocal microscopy after staining with rabbit anti-ovastacin
984 (green). Chromosomes were stained with DAPI (blue). The scale bar represents
985 10 μm. (**F**) MII oocytes and 2PN embryos from *Zip10*$^{f/f}$ and *Zip10*$^{d/d}$ mice were
986 imaged by BZ-X700 microscopy after staining with rat anti-mouse FR4 (JUNO;

987 green). Chromosomes were stained with DAPI (blue). The scale bar represents
988 10 μm.
989
990 **Movie legends**
991 **Movie 1. Monitoring of intracellular calcium ions during fertilization of**
992 ***Zip10$^{f/f}$* oocytes.** The changes in Ca^{2+} were detected by CalbryteTM 590 AM
993 every 4 second. *Zip10$^{f/f}$* oocytes displayed the calcium oscillations following
994 fertilization. The changes in zinc ions were also monitored simultaneously (Movie
995 2). The video was excerpted from maximum 50 min.
996
997 **Movie 2. Monitoring of extracellular zinc ions during fertilization of *Zip10$^{f/f}$***
998 **oocytes.** The changes in Zn^{2+} were detected by FluoZin-3 every 4 second.
999 *Zip10$^{f/f}$* oocytes released zinc ions into the extracellular environment through a
1000 zinc spark followed the first calcium rise following fertilization. The changes in
1001 calcium ions were also monitored simultaneously (Movie 1). The video was
1002 excerpted from maximum 50 min.
1003
1004 **Movie 3. Monitoring of intracellular calcium ions during fertilization of**
1005 ***Zip10$^{d/d}$* oocytes.** The changes in Ca^{2+} were detected by CalbryteTM 590 AM
1006 every 4 second. *Zip10$^{d/d}$* oocytes displayed the calcium oscillations following
1007 fertilization. The changes in zinc ions were also monitored simultaneously (Movie
1008 4). The video was excerpted from maximum 50 min.
1009
1010 **Movie 4. Monitoring of extracellular zinc ions during fertilization of *Zip10$^{d/d}$***
1011 **oocytes.** The changes in Zn^{2+} were detected by FluoZin-3 every 4 second.
1012 *Zip10$^{d/d}$* oocytes did not release zinc ions into the extracellular environment
1013 followed the first calcium rise following fertilization. The changes in calcium ions
1014 were also monitored simultaneously (Movie 3). The video was excerpted from
1015 maximum 50 min.
1016
1017 **Movie 5. Monitoring of intracellular calcium ions during parthenogenesis of**
1018 ***Zip10$^{f/f}$* oocytes.** The changes in Ca^{2+} were detected by CalbryteTM 590 AM

1019 every 4 second. *Zip10*$^{f/f}$ oocytes displayed a transient rise of calcium ions
1020 following artificial oocyte activation with ionomycin. The changes in zinc ions were
1021 also monitored simultaneously (Movie 6). The video was excerpted from
1022 maximum 50 min.
1023
1024 **Movie 6. Monitoring of extracellular zinc ions during parthenogenesis of**
1025 ***Zip10*$^{f/f}$ oocytes.** The changes in Zn^{2+} were detected by FluoZin-3 every 4
1026 second. *Zip10*$^{f/f}$ oocytes released zinc ions into the extracellular environment
1027 through a zinc spark followed a transient calcium rise following artificial oocyte
1028 activation with ionomycin. The changes in calcium ions were also monitored
1029 simultaneously (Movie 5). The video was excerpted from maximum 50 min.
1030
1031 **Movie 7. Monitoring of intracellular calcium ions during parthenogenesis of**
1032 ***Zip10*$^{d/d}$ oocytes.** The changes in Ca^{2+} were detected by CalbryteTM 590 AM
1033 every 4 second. *Zip10*$^{d/d}$ oocytes displayed a transient rise of calcium ions
1034 following artificial oocyte activation with ionomycin. The changes in zinc ions were
1035 also monitored simultaneously (Movie 8). The video was excerpted from
1036 maximum 50 min.
1037
1038 **Movie 8. Monitoring of extracellular zinc ions during parthenogenesis of**
1039 ***Zip10*$^{d/d}$ oocytes.** The changes in Zn^{2+} were detected by FluoZin-3 every 4
1040 second. *Zip10*$^{d/d}$ oocytes did not release zinc ions into the extracellular
1041 environment followed a transient calcium rise following artificial oocyte activation
1042 with ionomycin. The changes in calcium ions were also monitored simultaneously
1043 (Movie 5). The video was excerpted from maximum 50 min.
1044
1045
1046
1047
1048
1049
1050

1051

1052

1053

1054

1055

Fig. 1.

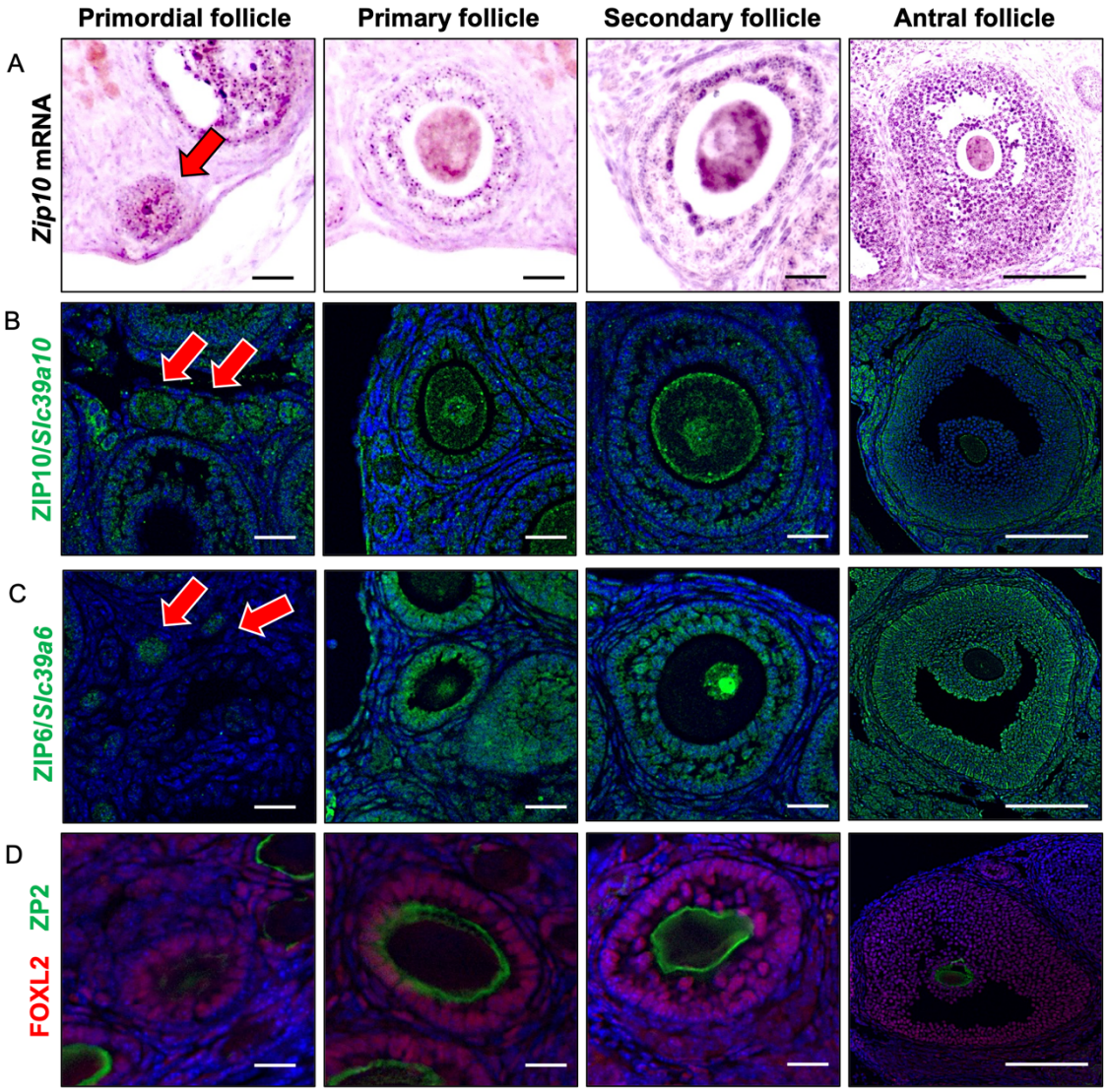

1056

1057

1058

1059

1060

1061

1062

1063

Fig. 2.

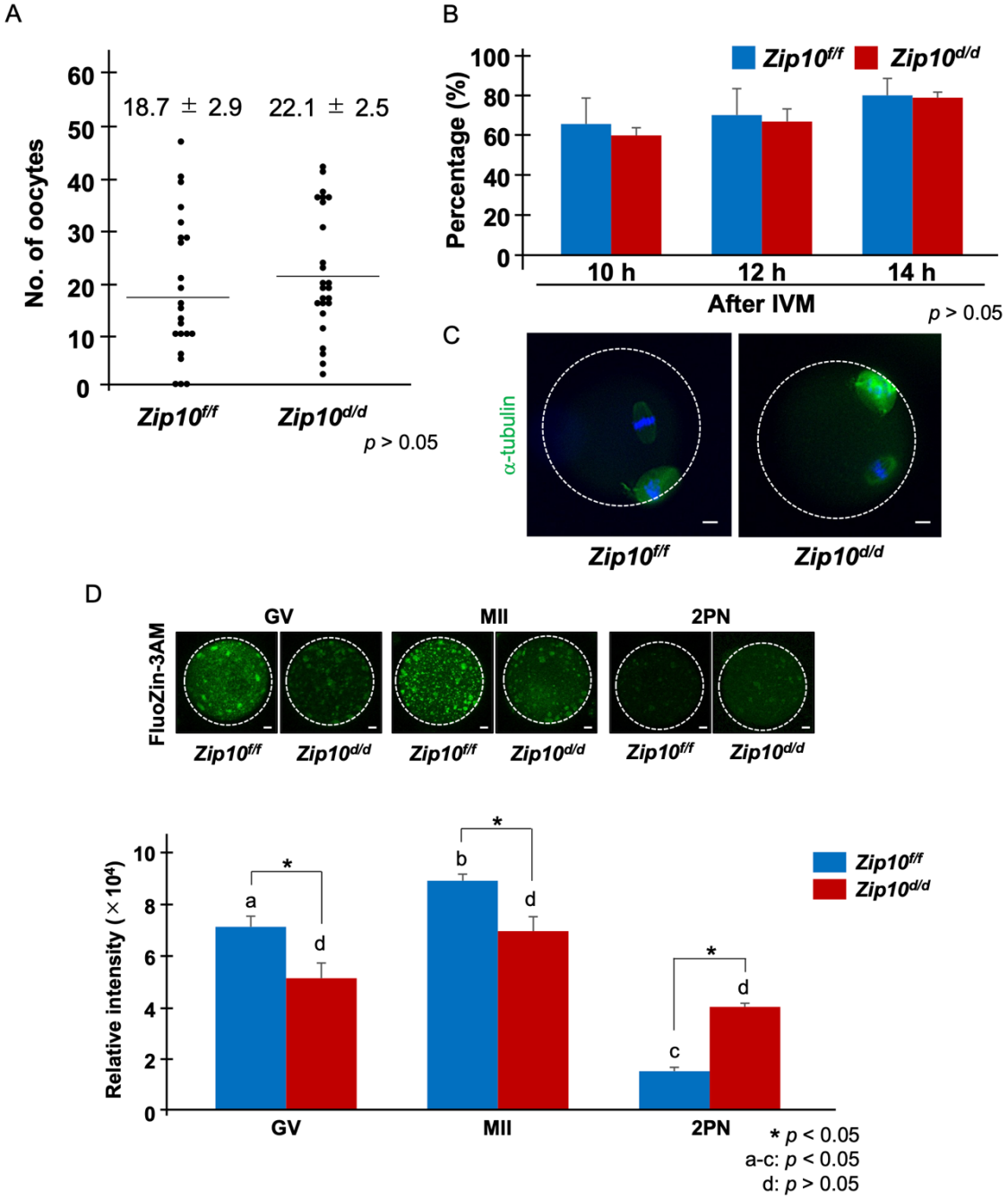

1064

1065

1066

1067

Fig. 3.

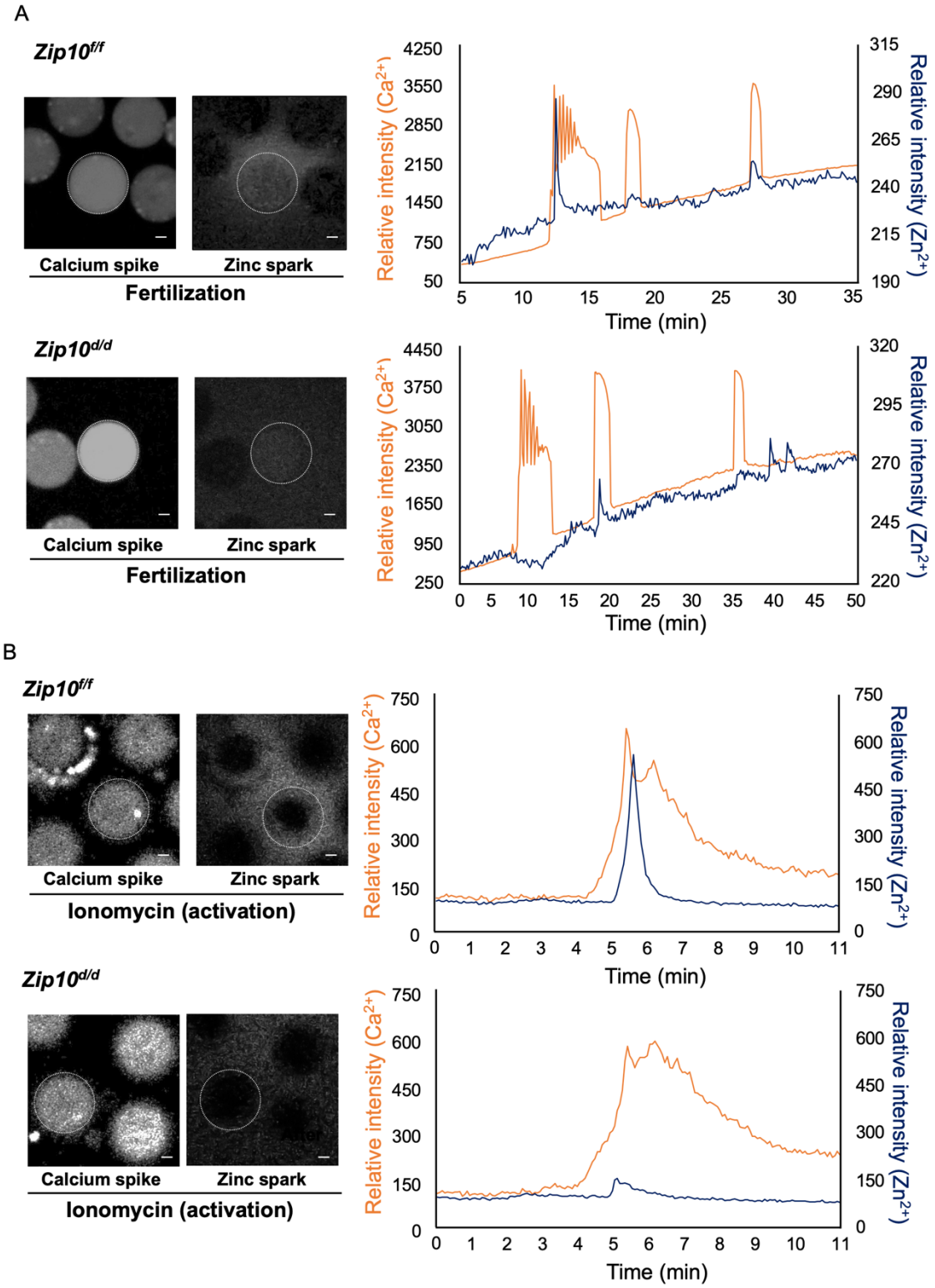

1068

1069

Fig. 4.

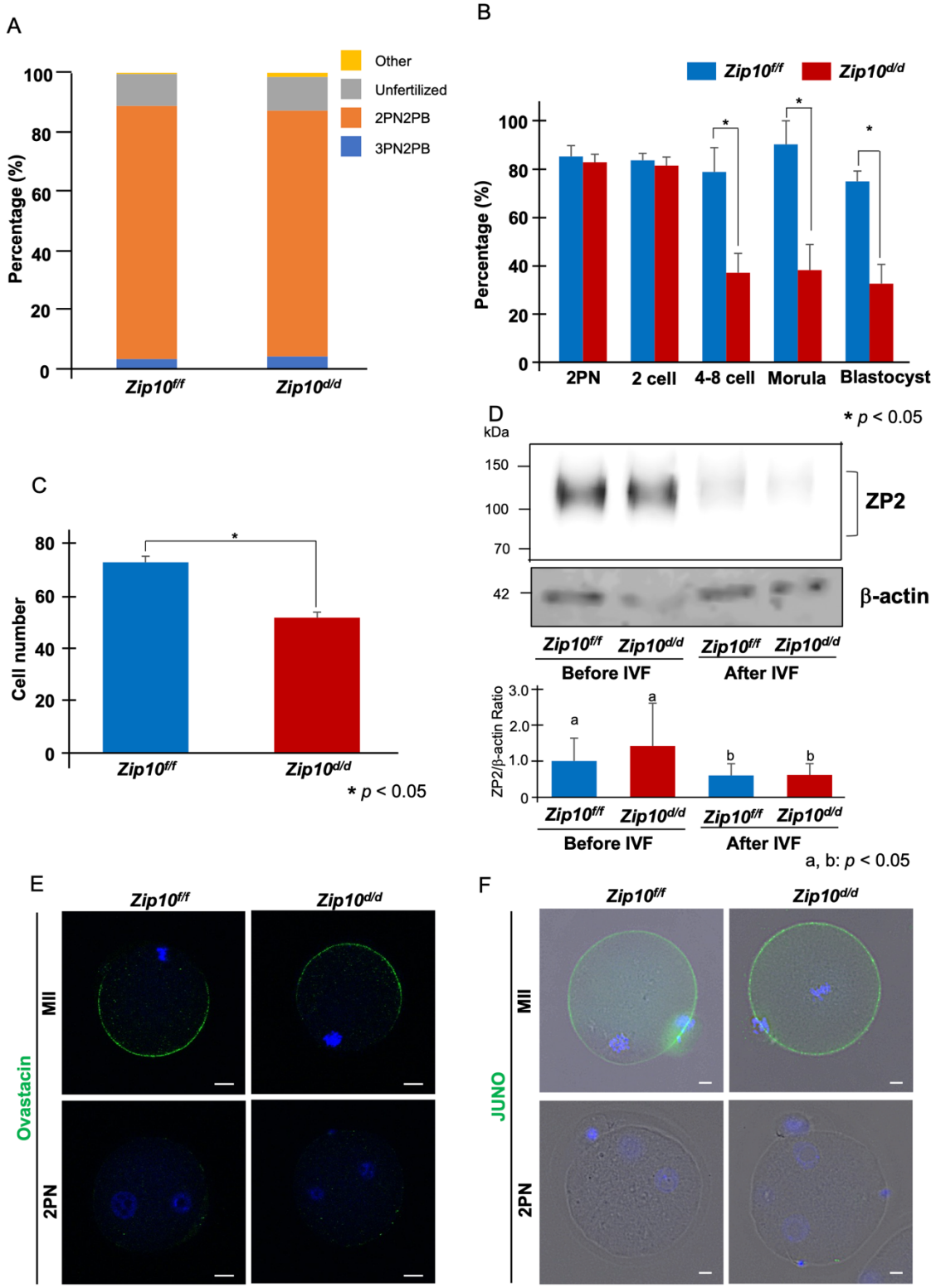

1070